Electronic Supplementary Material (ESI) for Dalton Transactions.

Supplementary Information

Graphene oxide encapsulated by mesoporous silica for intelligent anticorrosive coating: studies on release models and self-healing ability

Peng Du[a,b], Juan Wang[a], Haichao Zhao*[,a], Guangzhou Liu[b] and Liping Wang*[,a]

[a] *Key Laboratory of Marine Materials and Related Technologies, Zhejiang Key Laboratory of Marine Materials and Protective Technologies, Ningbo Institute of Materials Technology and Engineering, Chinese Academy of Sciences, Ningbo 315201, China.*

[b] *Institute of Marine Science and Technology, Shandong University, Qingdao 266200, China.*

■ **Elemental analysis**

In general, XPS is usually carried out to analyze of species and contents of compound in micro-areas composition of materials. The C 1s spectrum can be decomposed into three subpeaks, including C–C, C-O and O-C=O at 284.8, 285.7, and 288.1 eV, as shown in Figure S1.

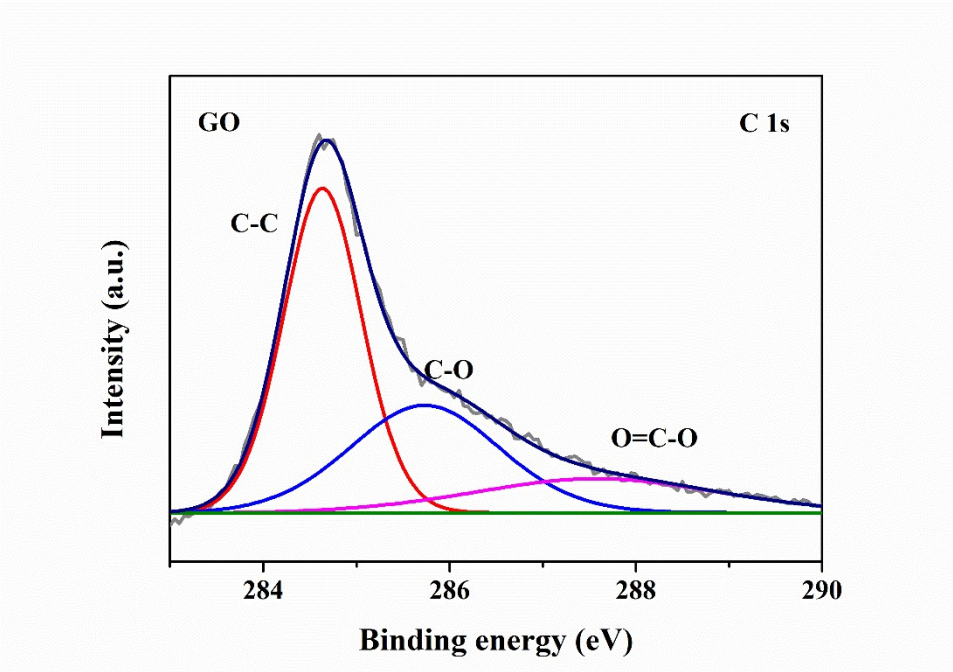

Figure S1. XPS High-resolution spectra of C in GO.

■ **Kinetic models of BTA from $mSiO_2$/GO nanoreservoir**

The release concentration, release rate and release percentage of BTA were recorded in and Figure S2. Nowadays, many of the commercial corrosion inhibitors were used to form a dense protective film on metal substrates. However, the inhibitor easily interacted with the coating system, which leaded the not only the failure and waste for inhibitor but also the defects and degradation for coatings. So it is necessary to study the release process of corrosion inhibitors leading to a higher efficiency in practical application from various nanocontainer. The obtained nanoreservoirs were explored especially in the pH factor triggering the release of BTA from the nanostructures. The release and release rate of benzotriazole increased with an

increase in the aqueous medium pH. The release rate gradually increased at the initial stage, then decreased, and finally got stabilized. Moreover, the release concentration reached the highest value of 6 mg/ (L· g nanocontainer) at around 300 min, close to 95%. This showed that the nanoreservoirs can effectively protect the corrosion inhibitor and improve the efficiency. BTA will not slow release too slowly to reduce the anti-corrosion capability, and will not release too quickly to damage the coating matrix. Further, the release amount was found to increase with an increase in the pH value from 3 to 11.

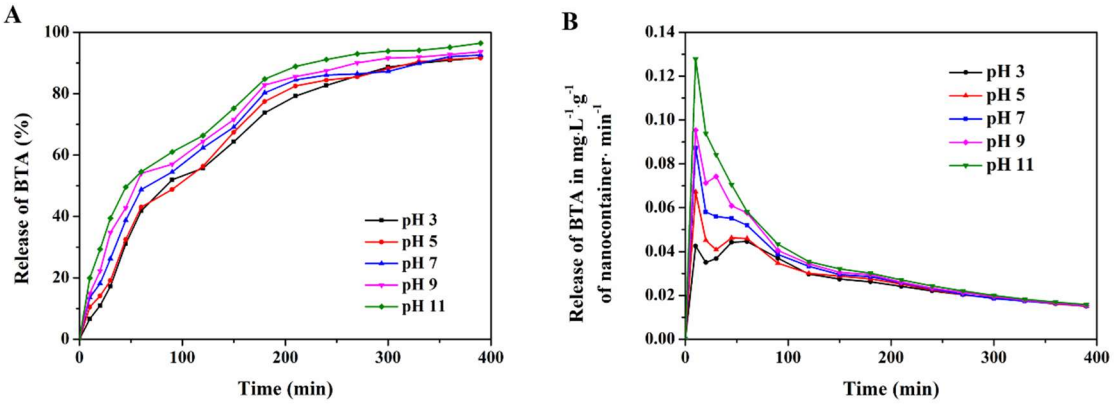

Figure S2. (A) Release percentage and (B) release rate of BTA from $mSiO_2$/GO nanoreservoir at different pH values.

The BTA release data at different pH values with respect to time was fitted to zero-order, first-order, Higuchi, Hixson–Crowell, Korsemeyer–Peppas and Hopfenberg models. Specially, the zero-order (1), first-order (3), Higuchi (4), Hixson–Crowell (5), Korsemeyer–Peppas (6) and Hopfenberg (7) models were carried out to make sure the release capacity at different pH values with respect to time. The selected models considered the pH changing and the structural changes of nanoreservoir will have changes, such as damage and dissolution. The kinetic models were displayed as following:

$$Q_0 + k_0 t = Q_t \quad (1)$$

it is assumed that the release rate of BTA has nothing to do with the accumulation of BTA, so Q_0 is the initial amount of BTA in the solution, k_0 is the zero-order release constant and Q_t is the amount of BTA released after time t.

$$dM/dt=kM \quad (2)$$

where k = first-order release constant. Combined with the Fick's first law, time integration is available as follow.

$$\ln(M_t/M_\infty) =-kt \quad (3)$$

where M_∞ = initial concentration of BTA in nanoreservoir, and M_t = concentration of BTA in nanoreservoir after t.

$$K_H t^{1/2}= Q_t \quad (4)$$

where Q_t is referred as the amount of BTA in solution with respect to time t, and K_H is denoted as the Higuchi dissolution constant. Higuchi model was often used to describe the sustained release of a water-soluble formulation from a semi-solid or solid matrix.

Hixson–Crowell kinetic model is usually used for understanding the matrix erosion mechanism during the release process. The equation can be expressed as:

$$W_0^{1/3}- W_t^{1/3}= K_s t \quad (5)$$

K_s is the kinetic constant of the Hixson-Crowell model. W_t and W_0 are cumulative amount of BTA in nanoreservoir system at time t and initial time, respectively. The Hixson-Crowell model is based on the Higuchi model. It was used in description of sustained release from a spherical matrix. Although the nanoreservoir is a lamellar structure, this model still has its research value due to the existence of mesoporous (similar to spherical) structure.

$$Q_t/Q = k_t t^n \quad (6)$$

where Q_t and Q_0 is the amount of BTA released after time t and the initial amount, respectively. In the model, k_t is the release rate constant, and n is represents to the release exponent. Moreover, (i) n = 0.45 is a typical Fick's diffusion; (ii) 0.45 < n < 0.89 is an irregular release (diffusion and polymer skeleton relaxation simultaneously); and (iii) n = 0.89, indicats a pure skeleton relaxation or dissolution-regulated release (zero-order kinetics)

$$1-(1-Q_t/Q_\infty)^{1/n}= kt \quad (7)$$

where Q_t and = Q_∞represent to the amount of BTA released after time t and at infinite time. Furthermore, k is the release rate constant, and n is representing to the release exponent (Because of the sheet structure, n=1 in this case). It should be noted that, n is shape factor, $n_{sphere} = 3$, $n_{cylinder} = 2$ and $n_{sheet} = 1$. When the carrier is a thin sheet, its release behavior follows a zero-order release process.

It is clear that the first-order kinetic release model shows a linear relation between ln (M_∞ /M_t) and ln t in the media and most fits the original data compared with other semiempirical model. The first-order release constant, a function of time t is found to be in the range of 0.0070 to 0.0092 min^{-1}. The rate constant values increased with an increase in the pH value from 3 to 11, which indicated that higher release content in the alkaline zone due to the surface negetive potential of BTA and nanoreservoir. resulting in significant anticorrosive performance. In this system, the release process of BTA obeyed the exponential rule and Fickian equation, which means the release rate is determined by the environment factor instead of the BTA concentration. So this nanoreservoir can achieve sustained and efficient release of corrosion inhibitor. And we can conclude that the first-order model is more valuable in practical anticorrosive application due to its simplicity and ease of use. Similarly, the fitting

results using zero-order, Hixon–Crowell, Higuchi, Korsmeyer–Peppas and Hopfenberg kinetics models were observed from Figure 5 and Table S1. Though they presented the similar trend in different pH values, we can intuitively observe different fitting results which present poor matching.

Zero-order release means that the release rate does not change with time, that is, the rate remains constant during the corrosion inhibitor release cycle. Further, because of the low degree of fitting, the model is not suitable for practical use. Higuchi model was often used to describe the sustained release from a semi-solid or solid matrix, especially the porous framework polymer system. This model is based on the Fickian diffusion theorem, but the fitting degree in the alkaline media is not very high, which may be due to partial dissolution of the mesoporous structure in the nanoreservoir under high pH conditions. The Hixson-Crowell kinetic model is derived from Fick's first law, but needs to consider nanoreservoir volume and weight changes. Although it has a high degree of matching under alkaline conditions, the fitting in acidic conditions and initial release stage is relatively poor. So we believe that this phenomenon is mainly caused by the surface potential rather than the massive dissolution of the nanoreservoir. From a holistic point of view, this model does not meet the requirements in practical applications. The Hopfenberg model shows exactly the same trend with zero-order model. We found that the nanoreservoir is considered as a 2D materials, so the shape factor is 0. The fitting results are fully consistent with the results caculated by zero-order model. Finally, we analyze the Korsemeyer-Peppas model. The degree of fitting is still higher in the alkaline zone, the diffusion index n at this time is less than 0.45, so it is mainly controlled by Fickian diffusion. However, in the acidic and neutral regions, the release mode

is the combination of Fickian diffusion and dissolution (controlled by zero-order model). In addition, the degree of fitting is not high than that of first-order model, so this is not the best model for BTA release in this system. Finally, we can conclude that the first-order model is more valuable in practical anticorrosive application due to its accurate, simplicity and ease of use.

■ **RMSE values in different models**

The root-mean-square error (RMSE) of a model prediction with respect to the estimated variable X_{model} is defined as the square root of the mean squared error:

$$\text{RMSE} = \sqrt{\frac{\sum_{i=1}^{n}(X_{expt,i} - X_{model,i})^2}{n}} \quad (8)$$

where n is the number of data, X_{expt} is observed values and X_{model} is modeled values. RMSE values of the model predictions of different models are reported in Table S1.

The RMSE value is relatively low when compared with the other models though higher than that of Hixon–Crowell and Korsemeyer-Peppas due to some extreme values. Therefore we could make sure that the first-order kinetic model reflecting the Fick's diffusion was the most accurate one to predict the corrosion inhibitor release process.

Table S1. Kinetic data for BTA release at different pH values.

pH	Zero order		First order		Higuchi		Hixson-Crowell		Korsemeyer-Peppas			Hopfenberg	
	k_0	R^2	k	R^2	K_H	R^2	K_s	R^2	k_t	R^2	n	K	R^2
3	0.0193	0.76	0.0070	0.99	0.3222	0.97	0.0031	0.95	0.0163	0.95	0.7140	0.0032	0.79
5	0.0195	0.72	0.0071	0.98	0.3266	0.97	0.0032	0.93	0.0265	0.97	0.6256	0.0032	0.76
7	0.0199	0.59	0.0073	0.96	0.3360	0.94	0.0033	0.89	0.0442	0.96	0.5360	0.0033	0.63
9	0.0204	0.48	0.0080	0.96	0.3472	0.95	0.0035	0.86	0.0600	0.96	0.4859	0.0034	0.53
11	0.0211	0.35	0.0092	0.97	0.3605	0.93	0.0038	0.86	0.0898	0.97	0.4170	0.0035	0.40
RMSE	1.2533		0.15884		0.4141		0.1198		0.1211			0.1996	

■ ζ-potential in different pH

It can be seen from the ζ-potential (Figure S3), as the pH increased, the surface protonation degree increased, so the release content got higher due to the increased repulsive force. Furthermore, when the material is in alkaline condition, BTA existed in the molecular form. Since the ζ-potential was negative, the surface of the $mSiO_2$/GO was negatively charged, which indicated that the OH- in the aqueous solution will develop the electrostatic repulsion with nanocontainer under alkaline conditions. So the release amount increased due to the certain damage to the nanostructure by alkaline.

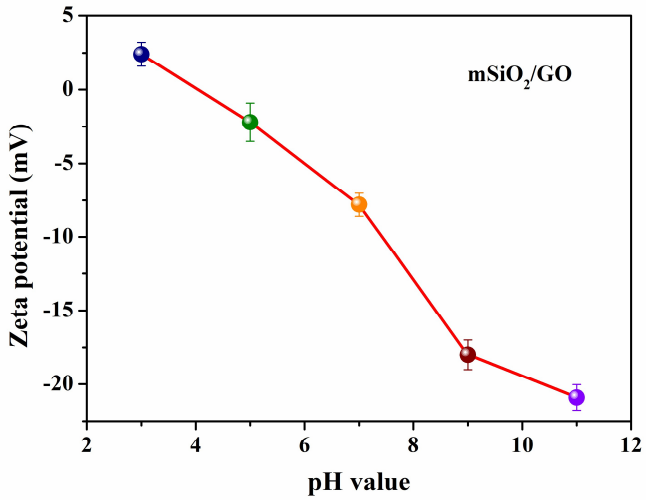

Figure S3. ζ- potential of $mSiO_2$/GO nanoreservoir at different pH values.

■ Surface wettability of the smart release coating system

The mild steel surface showed nanoreservoir repellent characteristics with a contact angle of 15.88°±1.2°, 18.76°±2.4° and 17.67°±1.3°. We noticed the difference was not so huge that methanol solution containing nanoreservoir had good adhesion to metals. As for the CS steel substrate recorded in Figure S4.

After the MG2 and MG3 coating on the PVB resin, the corresponding contact angle

increased to 27.73°±1.3°and 27.89°±1.3°, respectively. The higher improvement not only ensured the plasticity of the coating preparation but also preserved a significant mutual relationship of different layers.

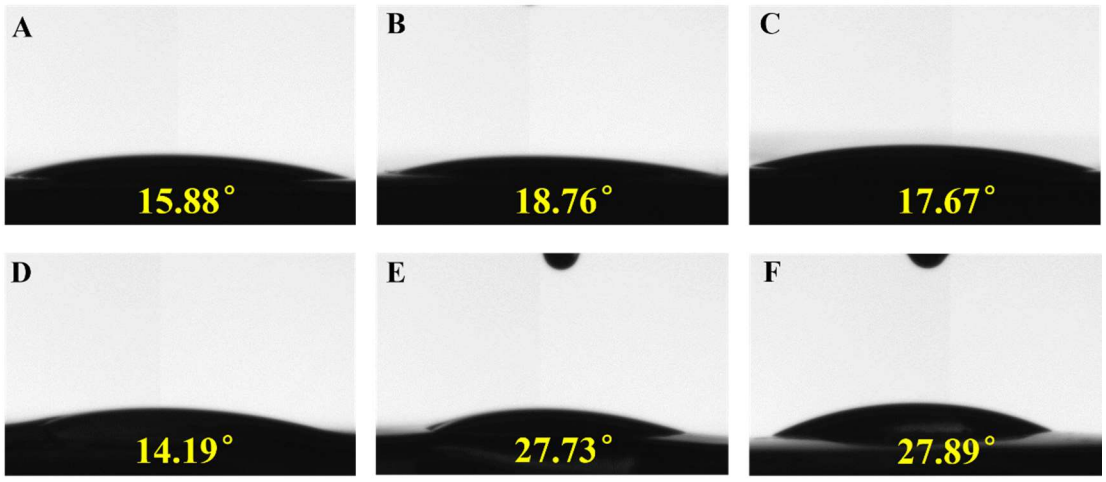

Figure S4. Contact angle measurement on the polished mild carbon steel surface and uncured PVB resin of different samples.

■ **The fitting data of the equivalent electric circuits**

The equivalent electric circuits (*EEC*) were also used to quantitative fit the EIS results by ZsimWin. After long term immersion, the coatings became permeable, so the inset *EEC* with a good agreement was used. As shown in Table S2, R_s, R_c and R_{ct} represented the solution resistance, coating resistance and charge transfer resistance, respectively. Further, because the electrochemical behavior was not in standard condition. The capacitors parameters should be substituted using a constant phase element (*CPE*) to obtain a real value, which was expressed by the following equation:

$$Z_{CPE} = \frac{1}{Y_0} \times \frac{1}{(j\omega)^n} \quad (9)$$

where Y_0 is the magnitude of the *CPE*, j is the imaginary unit, ω is the angular frequency , and n is the *CPE* exponent. When n=1, the *CPE* can be transferred into capacitance values.

Moreover, the *CPE* reflects the roughness of the electrode surface (Y_0) and the strength of the dispersion effect (n).

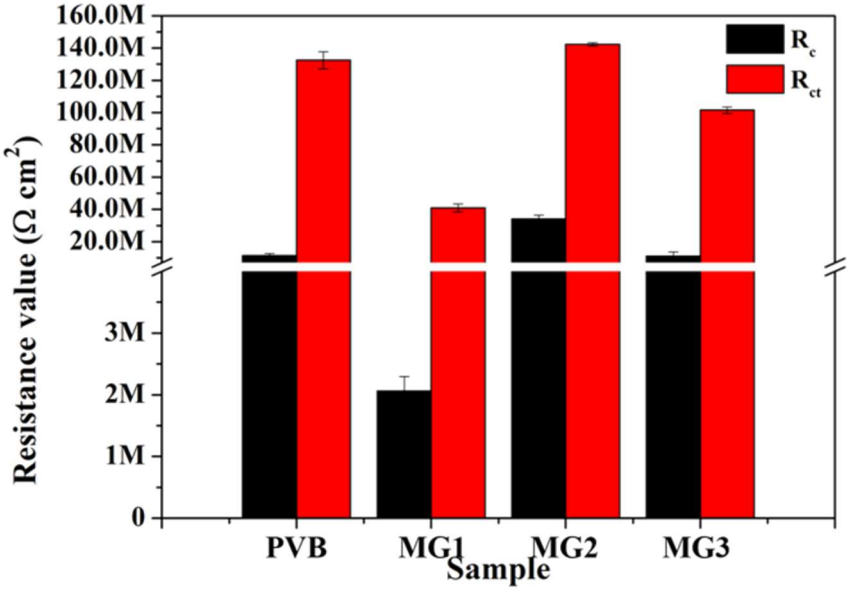

Figure S5. EIS fitting parameters for CS substrates with PVB, MG1, MG2 and MG3: evolution of coating resistance R_c with immersion in 3.5 wt% NaCl solution and charge transfer resistance R_c.

■ **Salt spray test after 10 days**

The salt spray test was performed to study the failure of coatings in practical condition. The specimens were exposed in a chamber with continuous spray and the changes were monitored. Visually, the pure PVB, MG1 and MG3 did not adhere well with the CS substrates after long-term test. Furthermore, massive red rusts were displayed for PVB and MG1 due to the weakened barrier function. The corrosion products generated and accumulated in the scratched area. It has also been seriously corroded in sample MG3. For sample MG2, although there were a small amount of corrosion products accumulated in the scratches, the amount of rust remained the constant after 10 days exposure due to the barrier of mSiO_2/GO and continuous release of BTA.

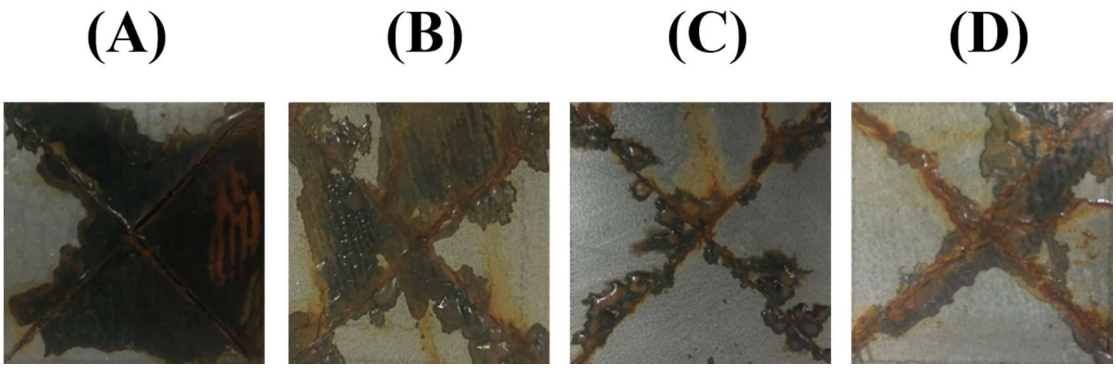

Figure S6. Digital images of the salt spray test after 10 days. (A) PVB; (B) MG1; (C) MG2; (D) MG3.

■ Anti-corrosion efficiency of the double layered coating system with BTA

All the electrochemical parameters were summarized in Table S2. The corrosion current density (i_{corr}), anodic Tafel slopes (β_a), and cathodic Tafel slopes (β_c) were calculated using the extrapolation of anodic and cathodic to the Tafel curves. The inhibition efficiency (η, %) were calculated by equation 10:

$$\eta = \frac{i^0_{corr} - i_{corr}}{i^0_{corr}} \times 100\% \quad (10)$$

Corrosion potential (E_{corr}) is a thermodynamic concept that reflected the tendency ofcorrosion reactions, so it is the uneasy to get corroded for anode metal covered with MG2. However, i_{corr} was a dynamic concept and was usually used to calculate the inhibition efficiency. As we obtained from Table S2, the highest η value of MG2 (99.99%) revealed the most reliable barrier performance.

Table S2. Fitting results of the potentiodynamic polarization of different samples.

Samples	E_{corr} (mV vs. SCE)	i_{corr}(A cm^{-2})	β_a(mV dec^{-1})	$-\beta_c$(mV dec^{-1})	R_{corr} (mm/year)	η (%)
bare steel	746	5.858×10^{-5}	83	112	-	-
PVB	609	8.040×10^{-8}	202	134	9.35×10^{-4}	99.86
MG1	597	6.825×10^{-8}	254	141	7.94×10^{-4}	99.88
MG2	425	3.225×10^{-9}	105	117	3.75×10^{-5}	99.99
MG3	525	1.780×10^{-8}	81	220	2.07×10^{-4}	99.97

Aggressive electrolytes and water gradually reached the metal through cracks or pores in the coatings. Therefore, a diffusion process appeared in the steel interfaces, indicating severe metal corrosion. So the EECs were used in Figure S6. Clearly, in Figure S6C, the R_c gradually decreased during immersion for 60 days. However, the coatings with BTA not only showed the highest R_c values, but also showed a slightly increasing trend. Figure S6D shows the instantaneous corrosion rate related values of R_{ct}. The values of R_{ct} in coatings with BTA were higher. The overall distribution of R_{ct} indicated that the coatings with BTA had a significant barrier effect and self-healability.

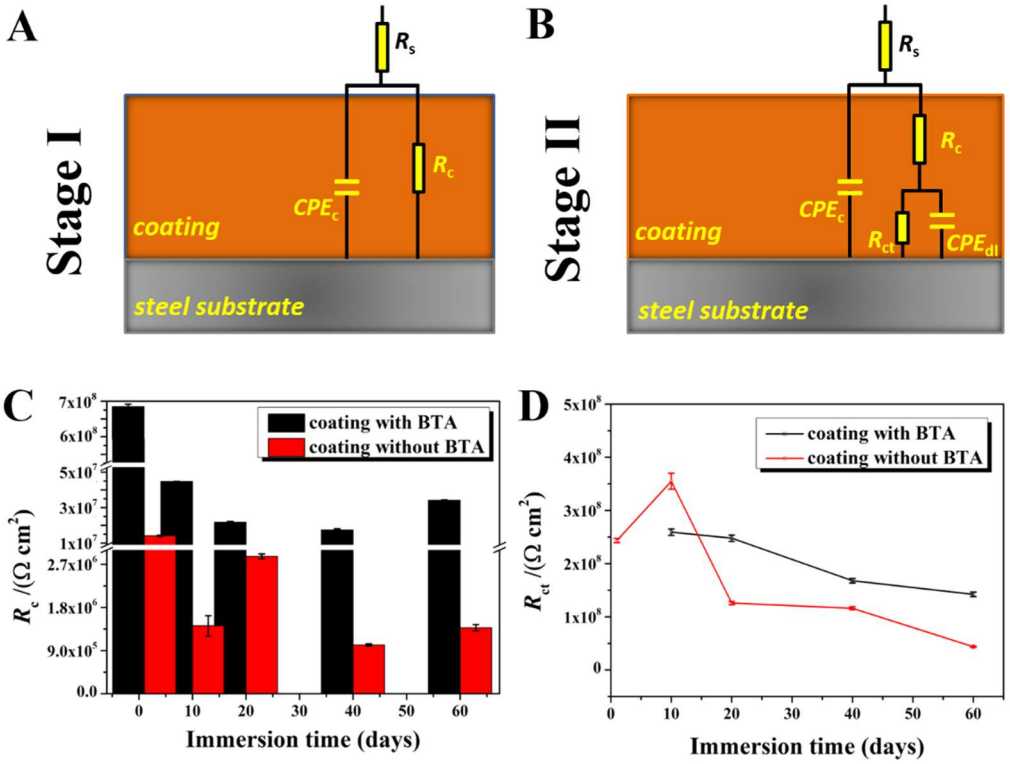

Figure S7. (A and B) Equivalent circuits used for EIS data fitting, (C) evolution of coating resistance R_c, and (D) evolution of charge transfer resistance R_{ct}.

References

1. Prasai, D.; Tuberquia, J. C.; Harl, R. R.; Jennings, G. K.; Bolotin, K. I., Graphene: Corrosion-Inhibiting Coating. *ACS Nano* **2012,** *6* (2), 1102-1108.

2. Ding, Y.; Wen, C.; Hodgson, P.; Li, Y., Effects of alloying elements on the corrosion behavior and biocompatibility of biodegradable magnesium alloys: a review. *Journal of Materials Chemistry B* **2014,** *2* (14), 1912-1933.

3. Ding, J.; Zhao, H.; Ji, D.; Xu, B.; Zhao, X.; Wang, Z.; Wang, D.; Zhou, Q.; Yu, H., Achieving long-term anticorrosion via the inhibition of graphene's electrical activity. *Journal of Materials Chemistry A* **2019,** *7* (6), 2864-2874.

4. Chang, K. C.; Hsu, M. H.; Lu, H. I.; Lai, M. C.; Liu, P. J.; Hsu, C. H.; Ji, W. F.; Chuang, T. L.; Wei, Y.; Yeh, J. M., Room-temperature cured hydrophobic epoxy/graphene composites as corrosion inhibitor for cold-rolled steel. *Carbon* **2014,** *66* (2), 144-153.

5. Xie, Z.-H.; Li, D.; Skeete, Z.; Sharma, A.; Zhong, C.-J., Nanocontainer-Enhanced Self-Healing for Corrosion-Resistant Ni Coating on Mg Alloy. *ACS Applied Materials & Interfaces* **2017,** *9* (41), 36247-36260.

6. Ding, J.; Zhao, H.; Wang, Q.; Dou, H.; Chen, H.; Yu, H., An ultrahigh thermal conductive graphene flexible paper. *Nanoscale* **2017,** *9* (43), 16871-16878.

7. Tyagi, M.; Bhanvase, B. A.; Pandharipande, S. L., Computational Studies on Release of Corrosion Inhibitor from Layer-by-Layer Assembled Silica Nanocontainer. *Industrial & Engineering Chemistry Research* **2014,** *53* (23), 9764-9771.